Ab initio derived augmented Tersoff potential for silicon oxynitride compounds and their interfaces with silicon

Salomon R. Billeter, Alessandro Curioni, Dominik Fischer,* and Wanda Andreoni
IBM Research, Zurich Research Laboratory, 8803 Rüschlikon, Switzerland
(Received 22 December 2005; revised manuscript received 2 March 2006; published 25 April 2006)

Coordination-dependent interatomic potentials are proposed for silicon oxides and oxynitrides—also hydrogenated ones—with a functional form based on the widely used Tersoff silicon potential. They are intended for an accurate sampling of the configurational space of realistic silicon oxynitride systems and their interfaces with silicon, including defects and changes of oxidation states. The parameters, which are given in the text, are obtained by simultaneously mapping forces and energies onto the results of density-functional-theory calculations performed for a set of diverse systems and configurations and a wide composition range. Application to a larger set of systems and configurations shows the transferability of these augmented Tersoff potentials and their validity in predicting bulk lattice parameters, energetics of defect relaxation, and vibrational spectra.

DOI: 10.1103/PhysRevB.73.155329 PACS number(s): 61.50.Ah, 68.35.−p

I. INTRODUCTION

Computer simulations are viewed as an increasingly useful tool for the investigation of real materials, the prediction of their physicochemical behavior, and ultimately the design of novel ones. Still, achieving a good compromise between accuracy and feasibility is a challenging issue for calculations based on atomistic models. Although systems of sizes in the nanometer scale have become affordable for *ab initio* calculations based on density-functional theory (DFT) (see, e.g., Ref. 1), the time scale of most dynamical processes of interest as well as the extension of configurational sampling required for a reliable search of equilibrium structures is still prohibitive. This is why building robust classical schemes for interatomic interactions is still a worthwhile effort for the simulation of real materials.

The purpose of this paper is to introduce a simple and at the same time highly transferable force field for SiON systems that is able to represent structural and dynamical properties for a wide range of compositions, in the bulk as well as at interfaces with silicon, and also in the presence of hydrogen. The target systems are large-scale models of interfaces and disordered phases; the target computational methodologies are molecular dynamics (MD) and Monte Carlo simulations of diffusion and growth processes, also combined with the replica-exchange method.[2] The efficient use of these procedures requires that the computation of both energies and forces be relatively inexpensive. In particular, at least the most demanding part of the evaluation of the energy should scale linearly, and a simple analytic expression is desirable for its gradient.

Our formulation is rooted on Tersoff's concept[3] of a local short-range potential for covalently bonded systems, in which the fundamental variable is an effective coordination depending on the local environment and the effects of a third atom are included as weakening of the attractive part of the two-body interaction terms. Previous applications of Tersoff's scheme to binary compounds of silicon with oxygen[4,5] and nitrogen[6,7] were limited in transferability and generally biased towards tetrahedral coordination for silicon. They were adjusted to represent a very limited data set derived from a mixture of experimental and computational results. The variety and complexity of the multinary systems we consider here impose a more substantial extension of the original expression[8,9] for the interactions between atoms of different elements and for a correct description of coordination changes and point defects, which inevitably form at the interfaces with silicon and, more generally, during processes like annealing and interdiffusion. For the sake of consistency and accuracy, the procedure we choose for optimization of the potential parameters consists in simultaneously fitting energies and forces to DFT values calculated for a selected set of systems in several different configurations, but to none of their physical properties. Our selection comprises a wide range of bonding situations, mostly in the condensed phase, which helps to enhance transferability further.

An exhaustive overview of the potentials proposed and applied to silicon and silicon dioxide in the past 30 years would exceed the scope of this work. Still it is imperative to mention that many other empirical potentials have been proposed for silicon and used to study a variety of properties (see, e.g., Refs. 10–15). We chose Tersoff's scheme because of its flexibility, the short range of the interatomic interactions, and its success in a wide range of applications to condensed phases (see, e.g., Refs. 8, 9, 16, and 17). For silica, a large variety of force fields have been used, including those based on the Keating[18,19] or Beest–Kramer–van Santen[20–22] (BKS) popular model and extensions[23] of the Stillinger-Weber formulation[10] for silicon, also involving fixed-charge Coulomb and polarizable charge-dipole interactions.[24] In particular, in Ref. 22, the BKS model was augmented with Morse-stretch bonds and fixed-charge Coulomb and induced-dipole interactions, and the parameters were adjusted to reproduce the energies, stresses, and forces calculated from high-temperature trajectories obtained with *ab initio* (DFT) MD simulations. A more flexible formulation was introduced in Ref. 25, in which atomic charges are allowed to change with the changing atomic environment according to the charge-equilibration procedure of Ref. 26.

The above models—and many others—have been applied to simulate the physical behavior of silica in its different phases (see, e.g., Refs. 27–30; for a recent critical review, see Ref. 31). SiO_2/Si interfaces, in contrast, have rarely been studied in classical MD or Monte Carlo simulations.[32–34] More often these methods are employed to generate the initial configuration of a DFT structural optimization.[35,36] A

study based on a refined Keating model[19,37] led to very interesting results for the structure and growth dynamics of the SiO_2/Si(100) system, some of which are consistent with a recent experiment.[38,39] However, this potential has inherent difficulties to describe other characteristics of the interface correctly.[40]

Fewer studies have been carried out for silicon nitride on the basis of classical MD simulations, generally based on force fields derived from those of silicon dioxide (see, e.g., Refs. 41–44). In particular, the potential of Vashishta *et al.*[24,45] has allowed very-large-scale, up to 10-million-atom, simulations and in particular of cracks formation at an interface between silicon nitride and silicon.[46] However, this scheme presents a serious drawback for the study of the dynamics of this complex interface, given that atoms are not allowed to change oxidation state and coordination number during a simulation.

After briefly reviewing the original expression of the Tersoff potential[9] for silicon and the characteristics of the Tersoff-derived potentials (Sec. II), we describe the procedure we followed to develop the new potential: namely, its extended formulation (Sec. III), the systems selected for the training set and the DFT calculations (Sec. IV), and the fitting procedure (Sec. V). In Sec. VI, all the parameters of the new force field are presented, accompanied by an evaluation of the fitting to the DFT data (Sec. VI A) and of their transferability. This is further tested against the DFT results on some properties of crystalline silicon dioxide and nitride—i.e., structural characteristics, defect relaxation energies, and vibrational properties. These results are compared with the predictions of other potentials and with experimental data (Sec. VI B). Additional details are given in the Appendixes. Appendix A lists the parameters of the "intermediate" potential schemes that we constructed starting from Tersoff and Tersoff-like potentials in Refs. 4, 6, 7, and 9. Appendixes B and C report further calculations performed for a vacancy in crystalline silicon and for the vibrational properties of silica and silicon nitride, respectively.

II. TERSOFF AND TERSOFF-DERIVED POTENTIALS

The expression of the Tersoff potential energy E of a covalent system composed of atoms like silicon, germanium, or carbon[8,9] is

$$E = \sum_i E_i = \frac{1}{2}\sum_{i\neq j} V_{ij}, \tag{1}$$

where the V_{ij}'s are generalized Morse potentials. Given a pair of atoms i and j, of elements I and J, respectively, their interaction V_{ij} is an explicit function only of their distance r_{ij},

$$V_{ij} = f_{ij}^{IJ}[A_{IJ}e^{-\lambda_{IJ}r_{ij}} - b_{ij}^{IJ}B_{IJ}e^{-\mu_{IJ}r_{ij}}], \tag{2}$$

where the function f_{ij}^{IJ} defines their action cutoff as

$$f_{ij}^{IJ} = \begin{cases} 1 & \text{if } r_{ij} \leqslant R_{IJ}, \\ \frac{1}{2}\left[1 + \cos\left(\pi\frac{r_{ij}-R_{IJ}}{S_{IJ}-R_{IJ}}\right)\right] & \text{if } R_{IJ} < r_{ij} \leqslant S_{IJ}, \\ 0 & \text{if } S_{IJ} < r_{ij}, \end{cases} \tag{3}$$

where R_{IJ} and S_{IJ} are appropriate cutoff radii. The coefficients A_{IJ} and B_{IJ}, the inverse decay lengths λ_{IJ} and μ_{IJ}, and the cutoff distances R_{IJ} and S_{IJ} depend only on the type of the two interacting atoms. When the two elements are the same, we will use only one index from now on: namely, e.g., $A_I = A_{II}$. For mixed covalent systems such as SiC, specific combination rules were given in Ref. 9:

$$A_{IJ} = (A_I A_J)^{1/2}, \quad B_{IJ} = (B_I B_J)^{1/2}, \tag{4a}$$

$$R_{IJ} = (R_I R_J)^{1/2}, \quad S_{IJ} = (S_I S_J)^{1/2}, \tag{4b}$$

and for the inverse decay lengths

$$\lambda_{IJ} = (\lambda_I + \lambda_J)/2, \quad \mu_{IJ} = (\mu_I + \mu_J)/2. \tag{5}$$

Three-body effects are incorporated into the damping factors b_{ij}^{IJ} of the two-body attractive interaction terms and depend on an "effective coordination number" $\beta_I\zeta_{ij}^{IJ}$:

$$b_{ij}^{IJ} = \chi_{IJ}[1 + (\beta_I\zeta_{ij}^{IJ})^{n_I}]^{-1/2n_I}, \tag{6}$$

where

$$\zeta_{ij}^{IJ} = \sum_{k\neq i,j} f_{ik}^{IK} e_{ijk}^{IJK} t_{ijk}^{I}. \tag{7}$$

The term t_{ijk}^I,

$$t_{ijk}^I = 1 + \frac{c_I^2}{d_I^2} - \frac{c_I^2}{d_I^2 + [h_I - \cos(\theta_{jik})]^2}, \tag{8}$$

incorporates the effect of the bending angle θ_{jik} between atoms j and k around atom i. In the original Tersoff potential for silicon,[8] the term e_{ijk} was designed to represent the fact that the influence of a third atom k on the i-j bond decreases, when the i-k distance becomes large compared with the i-j distance. However, in multicomponent systems, e_{ijk} is generally set to unity.[6,9]

$$e_{ijk} = \begin{cases} \exp[\mu^3(r_{ij} - r_{ik})^3], & \text{pure Si}, \\ 1, & \text{mixed systems}. \end{cases} \tag{9}$$

Note that, for a given i-j pair, both V_{ij} and V_{ji} are included in the total energy expression [Eq. (1)], but owing to the different bonding environments of the two atoms, they are not equal. The Tersoff potential in Eqs. (1)–(9) was originally designed for covalent systems. A straightforward extension to systems composed of atoms of significantly different electronegativity, such as silicon and oxygen, was believed to suffer from serious limitations. In the study of silica in Ref. 4, the Tersoff energy expression was extended to include an electrostatic potential and a self-energy term, with partial charges determined in a similar way as in the charge-equilibration method.[26] In addition, the term e_{ijk} was modified and set to

$$e_{ijk}^{IJ} = \exp[\mu_{IJ}^{m_I}(r_{ij} - r_{ik})^{m_I}], \tag{10}$$

thus including an additional integer parameter m_I, which was simply set to 1 for elements other than silicon. For silicon, the original value $m=3$ was kept. To our knowledge, this potential has not been used by other authors in its complete formulation; however, its parameters for the Tersoff-derived terms served as starting point for further refinement[5] and are part of commercial codes (see, e.g., Ref. 47).

The parameters for oxygen, nitrogen, and hydrogen were fitted in Refs. 4, 6, and 7, to reproduce a restricted database of known experimental and calculated properties of compounds containing these elements. In particular, the oxygen parameters were obtained from application to silica[4] as mentioned above. No precise indication was given about the reference data used, apart from those employed in the fitting of the electrostatic terms. Test calculations were presented for the properties of molecular oxygen and α-quartz, which, however, used the complete parameter scheme, including the electrostatic terms.

The data set used for nitrogen in Ref. 6 consisted of experimental values for the lattice parameter of β-Si_3N_4, the interatomic distance and the binding energy of the N_2 molecule, and of *ab initio* results for the average binding energy of β-Si_3N_4 and the structure of the Si_3NH_9 molecule. In the parametrization, the N-N attractive term was considered vanishing so as to avoid the formation of the dimer during simulations of the SiN_x systems.

Hydrogen parameters were fitted[7] to reproduce empirical values for the bond energy, the interatomic distance, and the vibrational frequency of H_2, the binding energy and equilibrium Si-H distance in SiH_4, and the structure of the $NH(SiH_3)_2$ molecule.

The starting point of our construction of an augmented Tersoff potential was the Tersoff potential itself for silicon[9] and the above-mentioned extensions for oxygen,[4] nitrogen,[6] and hydrogen.[7] These parameters are listed in Table II and referred to as the "Original" potential from now on.

In their construction of a Tersoff-like potential for silicon dioxide, Umeno *et al.*[5] fitted their parameters to DFT calculations, specifically via minimization of the root-mean-square mismatch of forces only. These computations used pseudopotentials obtained with the Troullier-Martins[48] method and a plane-wave basis set up to a cutoff of 22 Ry for silicon and 34 Ry for systems containing oxygen. Unfortunately in Ref. 5 no mention was made of the exchange-correlation functional there adopted. The reference systems were limited to bulk silicon, β-cristobalite, and an abrupt model of its interface with Si(100). To enable an analysis of the performance of the scheme of Umeno *et al.* in SiONH systems, we have used them in combination with those for nitrogen and hydrogen derived in Refs. 6 and 7, and consistently applied the combination rules in Eqs. (4) and (5) to construct the missing mixed parameters. The resulting parameter set is given in Tables XIII–XV of Appendix A and referred to as "Original(U)."

III. AUGMENTED TERSOFF POTENTIAL FOR SiONH SYSTEMS

Our search for a more general and accurate interaction scheme, still based on Tersoff's concepts, primarily relied on fitting to the results of DFT calculations, performed in the Perdew-Burke-Ernzerhof (PBE)[49] approximation of the gradient-corrected exchange-correlation functional, by means of a simultaneous minimization of the energy and the force mismatch[22] relative to a set of diverse atomic configurations of the SiONH systems. Our choice for these reference systems as well as the reference DFT calculations will be reported in Sec. IV. Here we describe and justify the modifications we made to the original Tersoff expression, especially for the interaction terms between atoms of different elements.

(A) Our tests revealed that the expression e_{ijk} in Eq. (10) led to inconsistent effective coordination numbers in mixed systems whenever the characteristic lengths and interatomic distances ranged over significantly different values, as is the case for substoichiometric silicon oxide or silicon oxynitride. This flaw can easily be fixed by measuring each interatomic distance with its own characteristic length,

$$e_{ijk}^{IJK} = \exp[(\mu_{IJ} r_{ij} - \mu_{IK} r_{ik})^{m_I}]. \tag{11}$$

In this way, one obtains a more physical value for the "effective coordination number" in Eq. (6) than with Eqs. (9) and (10), and better numeric stability than with Eq. (10).

(B) As pointed out in Ref. 5, the combination rules for the interaction parameters of dissimilar atoms [Eqs. (4) and (5)] do not allow a good parametrization of silicon-oxygen and silicon-silicon interaction terms simultaneously because of the different types of bonding involved. An improvement is obtained by carrying out the optimization for each pair of atom types independently.

(C) Given that our selected training set comprises a range of systems with different numbers of atoms and different elements (see Sec. V), the expression in Eq. (1) for the total energy was augmented by the core energies E_I^0 as

$$E = \sum_{i \neq j} V_{ij} + N_I \sum_I E_I^0, \tag{12}$$

where N_I is the number of atoms of the Ith element.

Using this functional form with the modifications (A)–(C) described above, we have obtained a first new set of parameters for Si, O, N, and H, which will be referred to as "α-ZRL" from now on.

(D) However, further modifications were necessary to better account for changes in the coordination and formation of defects, especially at the interface between silicon and its oxide and oxynitrides. In the expression of the Tersoff potential,[9] the energy changes due to the occurrence of overcoordination or undercoordination for silicon atoms are elegantly included in the damping factor b_{ij}^{IJ} of the attractive interaction through the dependence on the effective coordination number $\beta_I \zeta_{ij}^{IJ}$. However, in the case of an overcoordinated atom i and a fully coordinated atom j, only the interaction $1/2V_{ij}$ is damped in Eq. (1), whereas $1/2V_{ji}$ still corresponds to the interaction between two fully coordinated atoms. As we have verified, this lack of symmetry tends to favor the formation of defects at SiO_2/Si interfaces. To remedy this flaw, an additional penalty E_i^c for the occurrence of undercoordination and overcoordination was introduced:

$$E = \sum_{i \neq j} V_{ij} + N_I \sum_I E_I^0 + \sum_i E_i^c, \tag{13}$$

$$E_i^c = c_{I,1} \Delta z_i + c_{I,2} \Delta z_i^2, \tag{14}$$

where Δz_i denotes the deviation from the expected coordination number and is given by

$$\Delta z_i = \frac{z_i - z_I^0}{|z_i - z_I^0|} f_s(|z_i - z_I^0|), \tag{15}$$

$$z_i = \sum_{j \neq i} f_{ij}^{IJ} b_{ij}^{IJ}, \tag{16}$$

$$|f_s(z)| = \mathrm{int}(|z|) + \begin{cases} 0 & \text{if } |z| \leqslant z_T - z_B, \\ \frac{1}{2}\left[1 + \sin\left(\pi \frac{|z| - z_T}{z_B}\right)\right] & \text{if } z_T - z_B < |z| \leqslant z_T + z_B, \\ 1 & \text{if } z_T + z_B < |z|, \end{cases} \tag{17}$$

where z_T and z_B are independent of the specific atom and $\mathrm{sgn}(f_s(z)) = \mathrm{sgn}(z)$. In Eq. (14), the linear term in Δz_i differentiates undercoordination and overcoordination; the quadratic term prevents undercoordination from being favored. Note that the expected coordination numbers z_I^0 are not integer values because the bond strengths b_{ij}^{IJ} are included in the bond count for z_i. The switching function $f_s(z)$ prevents vibrations about the equilibrium positions from contributing. The values obtained for this new and augmented parametrization, which we denote as ZRL, are listed in Tables II–IV.

IV. TRAINING AND TEST SYSTEMS: DEFINITION AND *Ab initio* CALCULATIONS

As mentioned above, all parameters of the new force fields (both α-ZRL and ZRL) were fitted to simultaneously reproduce energies and nuclear forces obtained from DFT calculations, specifically in the PBE approximation[49] for the exchange-correlation functional. Neither additional DFT values nor empirical data were used. In the derivation of our schemes, the parameters of the original Tersoff potential for silicon[9] were kept close to their original values by imposing a specific constraint. The reference calculations employed the plane-wave pseudopotential scheme of the CPMD code,[50] and in particular Troullier-Martins norm-conserving pseudopotentials[48] and an energy cutoff of 80 Ry. The direct inversion in iterative subspace (DIIS) algorithm was chosen for direct wavefunction optimization.[51] For the condensed-phase systems, periodically repeated supercells (to be specified in each case) were used and the Γ point only was taken as representative of its Brillouin zone. For the molecular systems, the Poisson equation was solved using the Hockney algorithm.[52]

Table I reports the 18 systems used as reference for the fitting of the potential and for its testing, and the number of configurations considered for each of them. The systems chosen as reference comprise diamond silicon, β-silicon nitride, crystalline and amorphous samples of bulk silicon oxynitrides, both hydrogenated and not, and abrupt as well as highly defective models for the $SiO_2/Si(100)$ interface. SiO_xN_y compounds have stoichiometric composition $[y = 2(2-x)/3]$ and a nitrogen content $\xi = y/(x+y)$ varying from 4% to ~90%. Their geometries were optimized in our previous DFT study.[53] In addition, α-quartz and β-cristobalite, β-Si_3N_4, a large silicon cluster kept in the bulk structure by hydrogen passivation, and the cubosiloxane molecule were used for testing the potential only.

Ab initio calculations of both the energy and its gradient with respect to the internal coordinates were run for 10 584 configurations. This large number was needed to ensure that for each system the extracted subset used for the fitting of the potential parameters was large enough to cover a representative area of the configurational space. Globally, the resulting training set contained 207 configurations.

For systems (a)–(k) and (m)–(q) in Table I, the atomic configurations were derived from snapshots taken at equidistant time intervals over the trajectories of 21 classical MD runs driven by the Original potential. The temperature spanned a range from ~150 to ~600 K, and each run had a duration of ~2 ps, following a short steepest-descent geometry optimization. For systems (l), (r), and (s), the selected configurations correspond to predictions of intermediate versions of the potential whose energy and/or gradients exhibited a strong mismatch with DFT calculations. They were added to the training and control sets to better calibrate the interaction terms of our final potential [Eq. (13)] that explicitly penalize overcoordination and undercoordination.

V. FITTING PROCEDURE

The energy mismatch D_E between the DFT-PBE reference results (E_{DFT}) and the ones obtained with the classical potential to be optimized (E_{pot}) was defined as

$$D_E^2 = \frac{1}{N_{fr}} \sum_f^{N_{fr}} [E_{pot}(\mathbf{x}_f) - E_{DFT}(\mathbf{x}_f)]^2. \tag{18}$$

Similarly the mismatch D_F between the corresponding gradients with respect to the Cartesian coordinates $x_{i,d}$ of the ith atom (force mismatch) is defined as

$$D_F^2 = \frac{1}{3\sum_f^{N_{fr}} N_{at,f}} \sum_f^{N_{fr}} \sum_i^{N_{at,f}} \sum_d^3 \left(\frac{\partial}{\partial x_{i,d}} E_{pot}(\mathbf{x}_f) - \frac{\partial}{\partial x_{i,d}} E_{DFT}(\mathbf{x}_f) \right)^2, \tag{19}$$

where N_{fr} is the total number of configurations $\mathbf{x}_f$ of the f system and $N_{at,f}$ is the corresponding number of atoms. Note

TABLE I. Systems used for fitting and testing, their characteristics, number of configurations used, and MD sampling time (see text). I and II indicate two different configurations. In particular sample II of SiONH (6%) includes an H_2 molecule. SiO_2/Si(100) refers to both ideal abrupt interfaces and highly defected configurations.

Compound (N content)	State	Structure (sample)	No. atoms	Sampling time (ps)	No. configurations		Label
					Training	Control	
Si	solid	diamond	64	4	20	868	a
$Si_{123}H_{100}$	cluster	diamond	223	2		449	b
SiO_2	solid	α-quartz	72	2		500	c
	solid	β-cristobalite	192	2		499	d
Si_3N_4	solid	β-Si_3N_4	42	4	20	1000	e
$Si_8O_{12}H_8$	mol.	cubo-siloxane	28	2		500	f
SiON							
(4%)	solid	amorphous	71	2.2	20	849	g
(8%)	solid	with defects	62		1	1	h
(12%)	solid	amorphous	69	4	20	894	i
(16%)	solid	with defects	70		1	1	j
(40%)	solid	with defects	64	2	10	500	k
(94%)	solid	amorphous	170		2	2	l
SiONH							
(6%)	solid	amorphous (I)	76	4	20	1000	m
	solid	amorphous (II)	78	2	10	498	n
(8%)	solid	α-quartz	76	4	20	1000	o
	solid	amorphous (I)	73	4	20	1000	p
	solid	amorphous (II)	73	4	20	1000	q
SiO_2/Si(100)	solid	β-cristobalite	92		12	12	r
SiO_2Si(100)	solid	tridymite	100		11	11	s

that all N_{fr} configurations $\mathbf{x}_f$ were taken simultaneously to allow maximum transferability.

Minimization of only the energy error D_{E} delivers a good ordering for the energies of different configurations but a poor result for the forces at geometries near equilibrium. Indeed this procedure necessarily samples higher-weight regions of the potential energy surface, which are far from equilibrium. On the other hand, minimization of only the force mismatch D_{F}, while leading to a good prediction of the equilibrium geometries, results in a highly incorrect energetic ordering of different configurations (see, e.g., Ref. 5). Consequently, the force mismatch and energy error were optimized together using a weighted sum,

$$D_{\mathrm{W}} = w_{\mathrm{E}} D_{\mathrm{E}} + (1 - w_{\mathrm{E}}) r_{\mathrm{B}} D_{\mathrm{F}}, \tag{20}$$

where r_{B} is the Bohr radius and w_{E} is the weight attributed to the energy mismatch. Values of w_{E} in the range from $\sim$0.05 to $\sim$0.2 were found to provide a good trade-off between the prediction of the energy and forces.

The weighted error function D_{W} was locally optimized using the limited-memory Broyden-Fletcher-Goldfarb-Shanno (L-BFGS) method with line search[54] and steepest descent with a dynamic trust radius; its gradient with respect to the force-field parameters was calculated using finite differences. In addition, at different steps of the optimization, a global minimization of the force mismatch D_{F} was performed on the configurations of a few silicon oxynitride systems (Table I). A subspace-searching simplex method was used for this unconstrained optimization.[55]

According to standard procedures of force-field construction, constraints were imposed to maintain the values of the parameters to be optimized within their physically meaningful ranges. The cutoff distances R_{IJ} and S_{IJ} were kept fixed during the global minimization of D_{F}. Both numerical stability and transferability of the potential were tested on all control configurations (see Table I).

VI. RESULTS

The values of the parameters of the ZRL force field are given in Tables II–IV. Table II lists the individual coefficients in the Tersoff expression [Eq. (2)] and compares them with those of the Original potential (see Sec. II). Table III reports the deviation of the parameters of the mixed terms in the ZRL force field from the combination rules, Eqs. (4) and (5) Table IV quotes the parameters of the augmentation term [Eqs. (13)–(17)]. The intermediate parametrizations Original (U) and α-ZRL are reported in Tables XIII–XV of Appendix A.

TABLE II. Comparison of parameters of the Original and ZRL potentials (see text). Values are in eV, Å, and $Å^{-1}$.

	Silicon		Oxygen		Nitrogen		Hydrogen	
Parameter	Original	ZRL	Original	ZRL	Original	ZRL	Original	ZRL
A_I	1830.8	1803.79	3331.0	3331.06	6368.14	6368.21	86.7120	86.9235
B_I	471.18	471.195	261.2	260.476	511.760	511.205	43.5310	42.9815
λ_I	2.4799	2.62392	5.36	3.78336	5.43673	5.60181	3.7879	3.85393
μ_I	1.7322	1.88891	2.68	3.34402	2.70000	3.16170	1.9800	1.97047
R_I	2.70	2.44809	2.70	2.26069	1.80	1.75256	0.80	0.77985
S_I	3.00	3.08354	3.00	3.31294	2.10	2.41523	1.00	0.88641
β_I	1.0999×10^{-6}	1.0999×10^{-6}	2	1.0027	5.2938×10^{-3}	4.4422×10^{-3}	4	4
n_I	0.78734	0.78766	1	3.98638	1.33041	2.42635	1	1.00921
m_I	3	3	1	1	1	1	1	1
c_I	1.0039×10^{5}	1.0039×10^{5}	0	0[a]	2.03120×10^{4}	2.2955×10^{4}	0	0
d_I	16.217	16.21701	1	1	25.5103	24.78674	1	1
h_I	−0.59826	−0.56239	0	−0.52909	−0.56239	−0.52909	1	1
$\chi_{\mathrm{Si},I}$	1	1	1	1	0.67	1	0.78	1
$\chi_{\mathrm{O},I}$	1	1	1	1	1	1	1	1
$\chi_{\mathrm{N},I}$	0.67	1	1	1	0	1	0.76	1
$\chi_{\mathrm{H},I}$	0.78	1	1	1	0.76	1	1	1

[a]Although not restrained to zero, the value obtained from fitting was negligible.

A. Quality of the parameter fit

In this section, we analyze the quality of the results of the fitting in terms of (i) the energy error renormalized to the number of silicon atoms $N_{\mathrm{Si},f}$ in each configuration f [$D_{\mathrm{E,Si}}$ in Eq. (21)], (ii) the force mismatch D_{F} defined in Eq. (19), and (iii) the correlation coefficient C_F between the forces thus derived $\mathbf{F}_{\mathrm{pot},f}$ and the DFT values $\mathbf{F}_{\mathrm{DFT},f}$:

$$D_{E,\mathrm{Si}}^2 = \frac{1}{N_{\mathrm{fr}}}\sum_{f}^{N_{\mathrm{fr}}}\left(\frac{E_{\mathrm{pot}}(\mathbf{x}_f) - E_{\mathrm{DFT}}(\mathbf{x}_f)}{N_{\mathrm{Si},f}}\right)^2, \tag{21}$$

$$C_{\mathrm{F}} = \frac{\sum_f^{N_{\mathrm{fr}}}\langle \mathbf{F}_{\mathrm{pot},f}, \mathbf{F}_{\mathrm{DFT},f}\rangle}{\left[\sum_f^{N_{\mathrm{fr}}}\langle \mathbf{F}_{\mathrm{pot},f}, \mathbf{F}_{\mathrm{pot},f}\rangle\right]^{1/2}\left[\sum_f^{N_{\mathrm{fr}}}\langle \mathbf{F}_{\mathrm{DFT},f}, \mathbf{F}_{\mathrm{DFT},f}\rangle\right]^{1/2}}, \tag{22}$$

$$\mathbf{F}_{\mathrm{pot},f} = \left[-\frac{\partial}{\partial x_{i,d}}E_{\mathrm{pot}}(\mathbf{x}_f)\right]_{i,d}, \quad \mathbf{F}_{\mathrm{DFT},f} = \left[-\frac{\partial}{\partial x_{i,d}}E_{\mathrm{DFT}}(\mathbf{x}_f)\right]_{i,d}. \tag{23}$$

Table V contains the energy error. Note that the renormalization mentioned above enables a better comparison of the different systems. To analyze its origin, we have performed one further step of optimization; namely, we have fitted the core energies for each control set separately while retaining all other parameters fixed. The corresponding error $D_{\mathrm{E,Si}}^{\mathrm{cc}}$ (also renormalized) is reported in Table V. We emphasize that the absence of the core energy term in the Original and Original(U) potentials does not allow a consistent evaluation of the energy error. Table VI gives the quality of the force fitting. Inclusion of both the force mismatch and the force correlation coefficient in the evaluation allows a sensitive assessment of the accuracy of the predicted forces both near and far from equilibrium.

The poor performance of the Original(U) force field on all samples of silicon oxynitride is not surprising in view of the different independent sources of the parameters and the subsequent application of the combination rules, Eqs. (4) and (5). The energy error of our force fields drops considerably when the atom core energies are reoptimized, which shows that the main cause of discrepancy comes from keeping the core energies constant for all chemical environments rather than from an incorrect energy ordering of different configurations of systems with the same composition.

TABLE III. Coefficients of mixed terms [Eq. (2)] of the ZRL potential expressed in terms of their deviation from the combination rule in Eqs. (4) and (5). The values for the inverse decay lengths are given in $Å^{-1}$.

Parameter	Si-O	Si-N	Si-H	O-N	O-H	N-H
$A_{IJ}/(A_IA_J)^{1/2}$	1.04752	0.58647	1.52966	1.26527	0.99853	0.83424
$B_{IJ}/(B_IB_J)^{1/2}$	0.99978	1.10293	1.68173	1.00075	1.01274	0.97237
$\lambda_{IJ}-(\lambda_I+\lambda_J)/2$	0.74003	−0.73787	−0.15903	2.34383	1.03160	0.07480
$\mu_{IJ}-(\mu_I+\mu_J)/2$	−0.30051	−0.19843	0.22168	3.50573	−0.22005	0.21563

TABLE IV. Parameters of the augmentation term (no analog in Tersoff-derived potentials) of the ZRL interaction scheme [Eqs. (13)–(17)]. z_T=0.49751 and z_B=0.20039 for all elements. E_I^0 is given in eV.

Parameter	Si	O	N	H
E_I^0	−103.733	−432.158	−264.156	−13.174
z_I^0	3.70	2.80	1.75	1.00
$c_{I,1}^c$	−0.1238	−0.0038	−0.0868	0
$c_{I,2}^c$	0.2852	0.1393	0.2454	0

B. Prediction of physical properties

In this section, we investigate some of the physical properties of SiO_2 as a further test of the transferability of the force field. We stress again that, unlike the procedures commonly used to construct classical potentials for condensed matter systems, ours has only energies and forces as reference physical quantities but none of the properties. Therefore the results discussed here are a test of the predictability of specific features. Structural characteristics, vibrational spectra, and relaxation energies of point defects were calculated in the four potential schemes considered so far [Original, Original(U), α-ZRL, and ZRL] and compared with the predictions of the DFT-PBE scheme. All calculations with classical potentials were performed in supercells: namely, $2\times2\times2$ for silicon and the silica polymorphs, $1\times1\times3$ for silicon nitride. For comparison, DFT calculations were carried out in these supercells and in the unit cell of the periodic lattice using an appropriate sampling of the Brillouin zone. To be consistent with typical DFT calculations of crystalline phases, we report the latter as reference. Computations are made with the number of plane waves kept constant, equal to the one corresponding to the largest cell considered and to the energy cutoff chosen. The cutoff energy E_{cut} and the number N_k of **k** points in the irreducible Brillouin zone are given in the table for each case. We have verified that the differences obtained with the supercell computations are not significative. Furthermore, comparison is made with the results obtained using the Compass[56,57] force field, which is part of commercial codes (see, e.g., Ref. 47) and thus widely used in materials modeling.

TABLE V. Energy mismatch (in eV): the error functions $D_{\text{E,Si}}$ [Eq. (21)] and $D_{\text{E,Si}}^{\text{cc}}$ as explained in the text. The notations of the control sets are self-explanatory with components labeled as in Table I. "SiON-ld" and "SiON-hd" refer to samples with low and high density of defects, respectively. Note that configurations with a high density of defects are also included in "SiO_2/Si."

Control set (components)	Control quantity	New potentials	
		α-ZRL	ZRL
Si	$D_{\text{E,Si}}$	0.153	0.121
(a)	$D_{\text{E,Si}}^{\text{cc}}$	0.008	0.009
SiO_2	$D_{\text{E,Si}}$	0.176	0.125
(c,d)	$D_{\text{E,Si}}^{\text{cc}}$	0.075	0.032
OxN	$D_{\text{E,Si}}$	0.200	0.190
(c,d,e,f)	$D_{\text{E,Si}}^{\text{cc}}$	0.141	0.085
SiON-ld	$D_{\text{E,Si}}$	0.087	0.088
(g,m-q)	$D_{\text{E,Si}}^{\text{cc}}$	0.083	0.081
SiON-hd	$D_{\text{E,Si}}$	0.249	0.299
(h-l)	$D_{\text{E,Si}}^{\text{cc}}$	0.044	0.042
SiO_2/Si	$D_{\text{E,Si}}$	0.485	0.272
(r,s)	$D_{\text{E,Si}}^{\text{cc}}$	0.355	0.171
All	$D_{\text{E,Si}}$	0.148	0.147
(a–s)	$D_{\text{E,Si}}^{\text{cc}}$	0.148	0.147

TABLE VI. Force mismatch D_{F} (in eV/Å), and force correlation coefficient C_{F} defined in Eqs. (19) and (22), respectively. Labels as in Table V. Note that full correlation corresponds to C_{F}=1.

Control set (components)	Control quantity	Old potentials		New potentials	
		Original	Original(U)	α-ZRL	ZRL
Si	D_{F}	0.115	0.121	0.239	0.139
(a)	C_{F}	0.987	0.987	0.967	0.985
SiO_2	D_{F}	1.464	1.780	0.505	0.643
(c,d)	C_{F}	0.625	0.884	0.962	0.945
OxN	D_{F}	1.329	1.627	0.518	0.769
(c,d,e,f)	C_{F}	0.694	0.861	0.960	0.933
SiON-ld	D_{F}	2.313	2.053	0.784	0.841
(g,m-q)	C_{F}	0.423	0.771	0.910	0.904
SiON-hd	D_{F}	4.064	70.44	1.885	1.606
(h-l)	C_{F}	0.213	0.026	0.717	0.785
SiO_2/Si	D_{F}	1.450	1.227	1.140	1.007
(r,s)	C_{F}	0.563	0.675	0.543	0.582
All	D_{F}	2.656	15.01	1.729	1.072
(a–s)	C_{F}	0.428	0.142	0.655	0.849

Figure 1 shows the potential energy surfaces (PES's) in the space of the lattice parameters, calculated for silicon dioxide in three crystalline modifications and β-Si_3N_4. Each point corresponds to full relaxation of the internal coordinates. The Original PES dramatically fails to stabilize SiO_2 in the crystal structures considered here. In the Original(U) scheme, SiO_2 is unstable in the α-quartz structure and collapses near the experimental values of the lattice parameters. The improvement introduced by our procedure is evident. As expected, ZRL performs only slightly better than α-ZRL in this application. In our potential schemes and in PBE as well, the energy change corresponding to a simultaneous similar variation of the two lattice parameters is significantly smaller for α-quartz and α-cristobalite compared to β-quartz. This result is in agreement with the analysis of the anomaly of the elastic constants reported in Ref. 58. Such a flatness is enhanced in the description provided by the potentials, as a

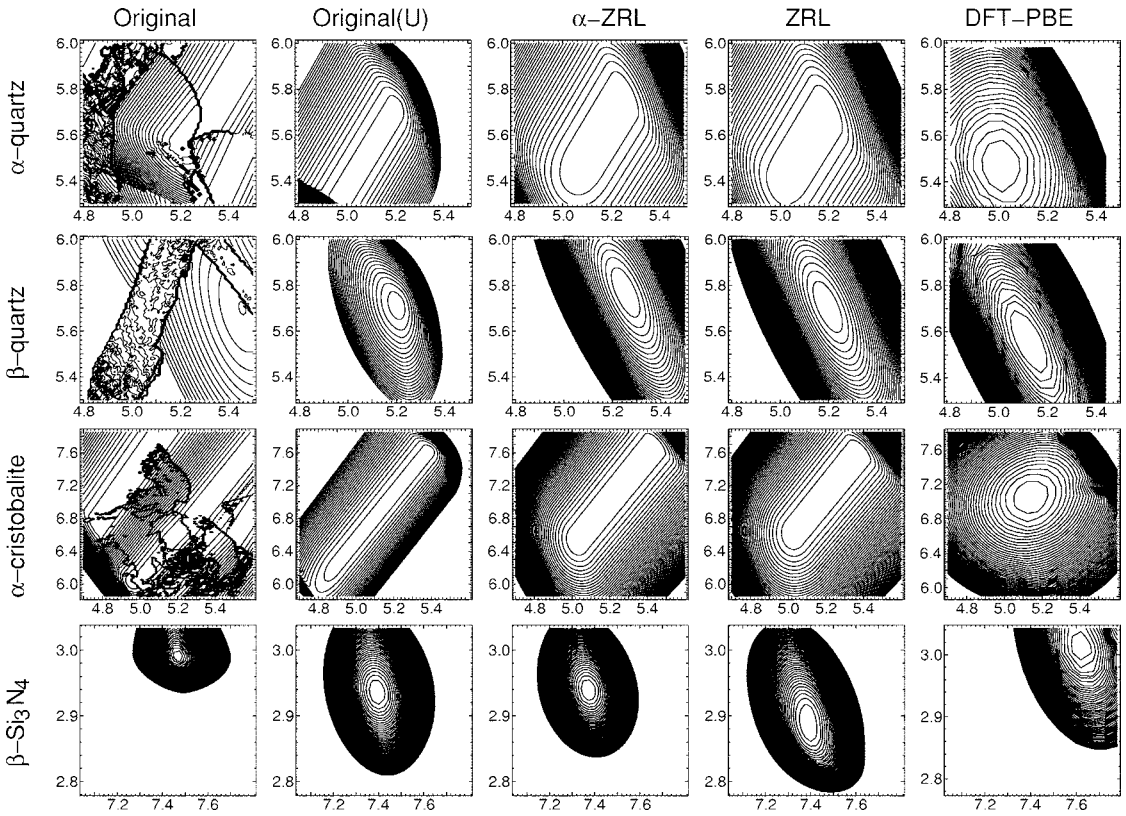

FIG. 1. PES calculated in the different classical potential schemes considered here and in DFT-PBE. Energies are in eV and distances in Å. The energy spacing is 0.005 eV for the three silica polymorphs and 0.0075 eV for the nitride.

consequence of their independence from bending around oxygen (c_O=0). This feature does not manifest itself in the case of β-quartz due to its different topology. We also note that in the Compass force field, α-quartz is metastable and easily transforms to β-quartz. The internal structure has a lower symmetry than expected from experimental data.

TABLE VII. Lattice parameters (in Å) calculated for bulk silicon, silicon dioxide, and silicon nitride. The uncertainty is indicated in brackets (see text). Missing values correspond to the cases where the structure is unstable (see Fig. 1 and text). The density ρ is given in g/cm^3.

			Old potentials		New potentials			
System	Property	Compass	Original	Original(U)	α-ZRL	ZRL	DFT PBE[a]	Exp
	a				5.16(12)	5.11(12)	5.019(28)	4.902[b]
α-quartz	c				5.62(20)	5.57(19)	5.472(45)	5.400[b]
	ρ				2.31(19)	2.38(19)	2.507(49)	2.664
	a	5.07		5.203(19)	5.255(27)	5.197(27)	5.134(59)	5.01[c]
β-quartz	c	5.59		5.714(27)	5.770(48)	5.707(49)	5.572(95)	5.46[c]
	ρ	2.41		2.234(27)	2.169(40)	2.242(43)	2.353(94)	2.52
	a	5.06		5.09(21)	5.23(23)	5.21(20)	5.131(71)	4.957[d]
α-cristobalite	c	6.83		6.90(74)	7.11(65)	7.10(57)	7.04(19)	6.890[d]
	ρ	2.28		2.23(43)	2.05(37)	2.07(33)	2.15(12)	2.357
	a	6.03	7.471(8)	7.395(13)	7.372(10)	7.388(19)	7.619(26)	7.608(5)[e]
β-Si_3N_4	c	2.23	2.991(3)	2.936(8)	2.939(6)	2.887(11)	3.015(16)	2.911(1)[e]
	ρ	6.63	3.222(10)	3.351(21)	3.368(16)	3.414(31)	3.084(37)	3.193(5)

[a]E_{cut} is 120 Ry. N_k is 14 for both quartz and cristobalite, and 27 for β-Si_3N_4.
[b]13 K, Ref. 64.
[c]600 °C, Ref. 65.
[d]10 K, Ref. 66.
[e]Room temperature, Ref. 67.

TABLE VIII. Structural energies (in kJ/mol) relative to α-cristobalite, with (E_{tot}) and without (E_{latt}) zero-point energy differences (see E_{ZPE}) in Table IX.

			Old potentials	New potentials		DFT	
System	Property	Compass	Original(U)	α-ZRL	ZRL	PBE[a]	Expt.
α-quartz	ΔE_{latt}			0.0	0.0	2.2	
	ΔE_{tot}			0.0	0.0	2.2	−3.41[b]
β-quartz	ΔE_{latt}	−2.3	−0.4	0.0	0.0	3.1	
	ΔE_{tot}	−3.1	−3.7	−0.5	−0.3	2.5	−2.94[b]

[a]N_k=47 and 40 for quartz and α-cristobalite, respectively. All other details as in Table VII.
[b]Ref. 68.

When applied to β-Si_3N_4, although one can find a minimum energy when the appropriate symmetry constraints are imposed on the lattice, the resulting internal structure does not preserve any symmetry.

Better agreement with the *ab initio* results is obtained when one focuses only on the equilibrium lattice parameters, whenever appropriate (see Table VII). In each case we quote the numerical uncertainty that we calculated; this is defined as the range of values in which the energy (per formula unit) does not vary within a given interval δE, which we chose as 0.001 eV for both the oxides and nitride. Moreover, control of this range of values provides a measure of the flatness of the PES around the minimum and of the relative difficulties inherent in any scheme. Partial comparison of classical potentials and *ab initio* and experimental data have been made (see, e.g., Refs. 25 and 59), which, however, did not account for the numerical uncertainty. The experimental data in Table VII refer to low temperature, whenever possible. Comparison with experiment also reveals the problems encountered by the *ab initio* approach, in particular the tendency of the PBE functional to predict lower atomic densities, which is not surprising. This tendency is further enhanced in the classical force fields we have derived, in the case of the silica polymorphs, while a substantial increase in the atomic density is predicted in the case of silicon nitride.

We performed the same calculations for silicon in the diamond structure. The PES is much less flat than in the oxide and nitride. If we choose a δE of 0.01 eV, the uncertainty in the determination of the lattice constant is less than 0.001 Å in all schemes. The original Tersoff potential accurately reproduces experiment (5.431 Å) by construction and so does ZRL [5.430(8) Å]. Original(U) results in a smaller lattice constant [5.379(7) Å], whereas the DFT-PBE and α-ZRL values are larger [5.467(7) and 5.680(5), respectively].

Structural energy differences are quoted in Table VIII and compared with the enthalpy changes measured at the structural transitions. The theoretical values include the zero-point energies that are determined from the spectrum of the long-wave vibrational modes calculated in the harmonic approximation, as described below. Although this comparison is interesting from a methodological point of view, we must emphasize that structural energy differences are much smaller than the error expected from a simple force field. Therefore, if such a force field successfully predicts this energy ordering—namely, in line with the relative thermodynamic stability of the different structures—this agreement must be considered fortuitous. On the other hand, it is noteworthy that the values of the zero-point energies (in Table IX) calculated with our potentials reproduce well the PBE values and their differences for all structures, while there is a strong discrepancy with the values obtained with other force fields. In Table IX, we also report an estimate obtained from the observed spectrum (TO modes), under the assumption that anharmonic effects are negligible.

The response of the system to the formation of a defect is of special relevance to the simulations of processing and growth of interfaces between heterogeneous materials. We considered the formation of an isolated vacancy of either silicon or oxygen in the α-quartz matrix. Table X contains the relaxation energy and the amount of structural relaxation

TABLE IX. Zero-point energies E_{ZPE} (in kJ/mol) calculated for different silica polymorphs in the optimized lattice (Table VII) and also in the experimental lattice of α-quartz.[a] The estimate from the observed vibrational spectra is also added (Expt).

			Old potentials		New potentials		DFT	
System	Lattice	Compass	Original	Original(U)	α-ZRL	ZRL	PBE	Expt.
α-quartz	optimized				27.0	29.0	27.9	
	experimental	33.5	23.4	43.7	29.9	31.1	28.0	29.4
β-quartz	optimized	32.4		35.7	26.5	28.7	27.3	
α-cristobalite	optimized	33.2		39.0	27.0	29.0	27.9	

[a]RT lattice parameters a=4.913 Å and c=5.405 Å.

TABLE X. Relaxation energies (in eV) of isolated vacancies in α-quartz and corresponding root-mean-square displacements (in Å) (see text). Labels as in Table VII.

		Old potentials		New potentials		
System	Vacancy	Original	Original(U)	α-ZRL	ZRL	DFT PBE
Si	E_{rel}	−3.627	−6.780	−0.701	−0.239	−0.221
	rmsd	0.175	0.433	0.126	0.107	0.057
O	E_{rel}	−2.523	−8.769	−1.128	−1.005	−1.008
	rmsd	0.175	0.399	0.150	0.141	0.104

involved. Calculations refer to a $(2\times2\times2)$ supercell, with lattice parameters kept at the optimum DFT-PBE value for the structure without defects. Therefore, these results are of interest only for the evaluation of the potentials versus the *ab initio* approach. The case of silicon is treated separately in Appendix B.

The ability to predict the vibrational properties of a given compound is generally a stringent test for a force field. Indeed given the realm of applications for which the potentials here proposed are intended, global characteristics and energetics like the zero-point energies mentioned above, are more important than the details of vibrational spectra of crystalline phases. Still, for the sake of completeness, we discuss them here both for α-quartz (Table XI) and β-Si_3N_4 (Table XII). Calculations were performed in the harmonic approximation, and the details were the same as those described for the structure optimization runs. In DFT-PBE we verified that the supercells used for the classical force fields were sufficient to reproduce the vibrational frequencies obtained with fully converged computations within one to two wave numbers.

Comparison with DFT-PBE results is significative because DFT-PBE provided the reference models in our fitting procedure. However, we also repeated these calculations in the structures corresponding to the equilibrium in each potential scheme. This allowed us to contrast our findings with those of other potentials in their equilibrium lattices. For the case of α-quartz, we report a comparison with the DFT-PBE spectrum. The changes at the equilibrium lattices were not significant. Although both are fitted to DFT forces and energies, the α-ZRL potential seems to reproduce the DFT spectrum better than the ZRL potential, especially in the high-frequency region. In particular, the gap between the bending and stretching modes is overestimated by more than 200 cm^{-1} in the ZRL scheme. The lowest and highest stretching E modes are inverted compared to DFT. This is consistent with the absence of the softening effect of the electronic polarizability in the potential schemes; the latter is indeed large only for one of the modes as shown by the LO-TO splitting. The analysis of the eigenvectors reveals discrepancies in the relative ordering of modes of different nature. One can then argue that, contrary to the assumption made in Ref. 31, a good representation of the phonon density of states is not sufficient for the evaluation of the accuracy of a potential scheme in describing the vibrational properties of this material. When constrained to the DFT-PBE cell of α-quartz, the Original(U) potential does not show an insta-

TABLE XI. Frequencies (in cm^{-1}) of long-wave vibrational modes of α-quartz calculated with DFT-PBE and with the different force fields in the PBE cell. The assignment refers to the irreducible representations of the point group D_3 (space group $P3_121$). E modes are both IR and Raman active; A_1 are Raman and A_2 are IR active. Experimental data are from Ref. 69 (IR) and Ref. 70 (Raman). "–" denotes the lowest E modes because not observed in IR spectroscopy.

Rep	Old potentials	New potentials		DFT	IR		Raman	
D_3	Original(U)	α-ZRL	ZRL	PBE	TO	LO	TO	LO
E	161	121	111	119	–	–	128	128
A_1	277	249	217	180			207	207
E	447	243	237	247	–	–	264.5	264.5
A_1	670	357	357	337			355	355
A_2	453	361	355	345	363.5	386.7		
E	557	362	354	371	393.5	402	394	403.5
E	782	472	456	417	450	510	450	508.5
A_1	840	501	474	435			464.5	464.5
A_2	696	452	452	460	495	551.5		
E	824	650	582	658	695	697.6	696	696
A_2	904	719	640	744	777	790		
E	994	740	661	758	797	810	796	809
E	1304	988	1245	1024	1065	1226	1067	1230
A_2	1267	988	1247	1027	1071	1229		
A_1	1324	997	1254	1041			1082	1082
E	1194	974	1191	1118	1158	1155	1159	1159

TABLE XII. Frequencies (in cm^{-1}) of the optically active long-wave vibrational modes of β-Si_3N_4 calculated with the new potentials in the corresponding optimized structures, and compared with DFT-PBE, experiment (Ref. 71) and the results of the Hessian-biased potential (WG) in Ref. 41. Our assignment refers to the irreducible representations of the point group C_{6h} (space group $P6_3/m$). Note however that in Ref. 41 the modes belonging to the E_{2g} and E_{1g} representations are not distinguished but all denoted as E_g.

Rep		Old potential	New potentials		DFT	
C_{6h}	WG	Original	α-ZRL	ZRL	PBE	Expt.
E_{2g}	190	319[a]	286	177	175	144
A_g	236	169	159	172	197	186
E_{1g}	215	480	257	207	218	210,229
E_{2g}	518	737[a]	464	420	431	
A_g	289	383	420	415	438	451
E_{2g}	592	996[a]	719	568	595	619
A_g	539	1730	934	825	700	732
E_{1g}	975	1230	935	1061	838	865
E_{2g}	1017	1231[a]	1012	1083	898	928
A_g	547	1207	998	1108	904	939
E_{2g}	1067	1737[a]	956	939	1004	1047
A_u	548	373	415	399	361	380
E_{1u}	481	394	434	423	413	447
E_{1u}	580	1012[a]	689	576	550	580
A_u	1062	1217	930	1064	828	910
E_{1u}	1012	1207[a]	1015	1095	859	985
E_{1u}	1064	1641[a]	958	1016	991	1040

[a]Unclean projection.

bility of the internal structure. In contrast, the Original potential results in a strong distortion such that the vibrational modes could no longer be classified according to the representations of the D_3 point group.

For the case of β-Si_3N_4, the computed spectra of the optically active vibrational modes in Table XII refers to the optimized lattices, and are compared to the prediction of a well-known "Hessian-biased" force field[41] and to experiment. Regarding our potentials, again more significant discrepancies are found in the frequencies of the stretching modes, which are also more strongly dependent on the lattice parameters. Still, the agreement is clearly better than that found with the Hessian-biased force field. This is also true when compared with other model potentials, which were either fitted to reproduce some undefined "dynamical properties"[60] or derived from DFT calculations performed in the local-density approximation.[61]

VII. CONCLUSIONS

In conclusion, we have developed a force field that is based on the Tersoff potential for covalently bonded systems, but modifies and augments it to enable a better description of mixed compounds and to account for the presence of coordination defects. In particular, it is tailored to accurately represent systems composed of silicon, nitrogen, oxygen, and hydrogen in noncrystalline phases, where a variety of chemical bonding situations are present. For this reason, the parameters were systematically fitted to simultaneously reproduce both forces and potential energies, for diverse configurations of a number of systems (mostly in the solid state), calculated in the framework of density-functional theory.

Although retaining the simplicity of a local potential, with focus on atomic coordination as predominant variable in determining the system energetics and atomic dynamics, the ZRL scheme necessarily includes a larger number of parameters to be fitted. However, the gain in accuracy and transferability is worthwhile, as shown in a number of applications, for which dramatic improvement was obtained over previous potentials of the Tersoff family as well as the Compass force field, which is widely used for modeling of the type of materials studied here. It is worth stressing that given the focus of our work on a global and comprehensive description of mixed SiONH compounds, the ZRL potential was not optimized to represent either one specific system, such as SiO_2 or Si_3N_4, or specific properties, such as vibrational spectra of crystalline phases. Still the comparison we have drawn also shows an improvement on the predictions of well-known force fields. Moreover and more importantly, unlike current non–*ab initio* approaches, the ZRL scheme allows a reliable description of changes in the bonding pattern that take place at the interface between silicon and its oxides and oxynitrides. Examples of successful applications to the study of SiO_2/Si(100) and SiON/Si(100) interfaces can be found in Refs. 62 and 63. In particular, in the SiO_2/Si(100) system, our scheme was able to predict the formation of a substoichiometric region and its characteristics in agreement with experiment[62] and to shed light on the major effects of the nitridization process.[63]

We must emphasize that the good performance of the ZRL potential in systems with partially ionic bonding is possible because the short-range terms of the electrostatic interactions, which are crucial for a correct description of different coordination environments, are implicitly accounted for. For this to be the case, the long-range behavior of the interatomic interactions should not be determined by monopole-monopole coupling. On the other hand, the short-range nature of our potential is instrumental in extending the time scale accessible to simulations.

Given the complexity of the interatomic interactions in the systems we have studied here, one cannot expect that a simple classical potential scheme is as accurate as *ab initio* calculations. However, being derived from DFT calculations without additional constraints, the ZRL force field can be reliably used in the modeling of large-scale, complex, and heterogenous systems, in combination with DFT-based MD simulations.

APPENDIX A: INTERMEDIATE PARAMETRIZATION SCHEMES

For the sake of completeness, we report here (Tables XIII–XV) the parameter sets obtained at intermediate steps of our study, as described in Secs. II and III.

TABLE XIII. Comparison of the parameters of the Original(U) potential and the corresponding ones in the α-ZRL potential. Values are in eV, Å, and Å^{-1}.

	Silicon		Oxygen		Nitrogen		Hydrogen	
Parameter	Original(U)	α-ZRL	Original(U)	α-ZRL	Original(U)	α-ZRL	Original(U)	α-ZRL
A_I	11422.0	1830.80	3439.0	3331.06	6368.14	6368.21	86.7120	86.9230
B_I	120.0	471.175	228.0	260.477	511.760	511.205	43.5310	42.9845
λ_I	3.94	2.45918	4.23	3.75383	5.43673	5.59852	3.7879	3.85415
μ_I	1.61	1.76191	1.01	3.35421	2.70	3.14828	1.98	1.97002
R_I	2.70	2.44810	2.70	2.26069	1.80	1.75256	0.80	0.77985
S_I	3.00	3.08355	3.00	3.31294	2.10	2.41522	1.00	0.88641
β_I	1.13×10^{-6}	1.0999×10^{-6}	1.86	0.28010	5.2938×10^{-3}	4.4422×10^{-3}	4	4
n_I	0.821	0.78665	0.151	0.75469	1.33041	2.42635	1	1.00921
m_I	3	3	1	1	1	1	1	1
c_I	1.06×10^{5}	1.0039×10^{5}	0	0[a]	2.03120×10^{4}	2.2955×10^{4}	0	0
d_I	15.4	16.21697	1	1	25.5103	24.78455	1	1
h_I	−0.317	−0.59912	0	0.96783	−0.56239	−0.53957	1	1
$\chi_{\mathrm{Si},I}$	1.00	1	1.00	1	0.67	1	0.78	1
$\chi_{\mathrm{O},I}$	1.00	1	1.00	1	1.00	1	1.00	1
$\chi_{\mathrm{N},I}$	0.67	1	1.00	1	0.00	1	0.76	1
$\chi_{\mathrm{H},I}$	0.78	1	1.00	1	0.76	1	1.00	1

[a]Not restrained to zero. The value obtained from the fitting was vanishingly small.

TABLE XIV. Coefficients of mixed terms [Eq. (6)] of the Original(U) and α-ZRL potentials, expressed in terms of the deviation from the combination rule of Eqs. (4) and (5). The values are given in Å^{-1}.

	Si-O		Si-N	Si-H	O-N	O-H	N-H
Parameter	Original(U)	α-ZRL	α-ZRL	α-ZRL	α-ZRL	α-ZRL	α-ZRL
$A_{IJ}/(A_IA_J)^{1/2}$	0.35552	1.04753	0.58647	1.52969	1.26527	0.99854	0.83424
$B_{IJ}/(B_IB_J)^{1/2}$	3.43613	1.00000	1.10301	1.68153	1.00075	1.01275	0.97236
$\lambda_{IJ}-(\lambda_I+\lambda_J)/2$	−0.52001	0.67692	−0.60402	−0.10789	2.37154	1.04786	0.08200
$\mu_{IJ}-(\mu_I+\mu_J)/2$	0.76000	−0.43480	−0.08761	0.25083	3.50485	−0.22886	0.22572

TABLE XV. Core energies (in eV) introduced in the expression, Eq. (12), of the α-ZRL scheme.

Parameter	Si	O	N	H
E_I^0	−103.8161	−429.7459	−263.3069	−12.7355

TABLE XVI. Relaxation energy (in eV) of an isolated vacancy in diamond silicon and corresponding root-mean-square displacements (in Å), calculated with a different choice of the lattice constant (see text). DFT-PBE and OPT denote the optimum values in PBE and in the corresponding force field respectively.[a]

		Old potentials		New potentials		DFT
Quantity	Lattice	Original	Original(U)	α-ZRL	ZRL	PBE
E_{rel}	PBE	−0.504	−0.062	−0.184	−0.358	−0.153
rmsd	PBE	0.050	0.020	0.039	0.051	0.064
E_{rel}	OPT	−0.388	−0.002	−0.232	−0.266	−0.153
rmsd	OPT	0.043	0.003	0.093	0.043	0.064

[a]For the sake of clarity, we repeat here the values reported in the text: 5.433 (Original), 5.379 [Original(U)], 5.680 (α-ZRL), 5.430 (ZRL), 5.467 (PBE) Å.

APPENDIX B: SILICON VACANCY

In analogy to the calculations presented in Table X, here we report (Table XVI) the results obtained for the relaxation of an isolated vacancy in silicon. In this case the comparison with the original potential is particularly interesting; therefore, we also quote the values calculated in the specific equilibrium structures. While PBE, ZRL, and Original agree in predicting a weak relaxation of the internal structure, the relaxation energies differ significantly. Note again that no optimization of the lattice constant of the model including the defect was attempted.

APPENDIX C: MORE ON VIBRATIONS

For a comparison with predictions from the Compass force field, we have to resort to the β-quartz structure (Table XVII), because in the α modification SiO_2 turns out to be unstable also when constrained to the DFT-PBE cell. In the β-quartz structure, Compass predicts a symmetry lowering. A sign of instability was found in the DFT-PBE scheme, marked by an imaginary frequency. We verified that the related eigenvector corresponds to the transformation from β to α-quartz. Indeed β-quartz is stable only at high temperature. In the α-ZRL and ZRL schemes, this is a soft mode (10 cm^{-1}). However it is very sensitive to small changes of the lattice parameters. For example, calculations performed in the DFT-PBE lattice with our potentials also predict an imaginary frequency.

TABLE XVII. Frequencies (in cm^{-1}) of long-wave vibrational modes of β-quartz calculated with lattice parameters optimized for each scheme. The assignment refers to the irreducible representations of the point group D_6 (space group $P6_422$). Note that in the Compass structure the vibrational modes could only be classified according to the representations of the C_6 point group. "—" indicates imaginary frequency.

		Old potentials	New potentials		DFT
Rep D_6	Compass (C_6)	Original(U)	α-ZRL	ZRL	PBE
B_1	55 (B)	—	10	10	—
E_1	107(E_1)	94	77	75	82
E_2	310(E_2)	433	245	238	234
B_1	352 (B)	533	350	343	342
B_2	416 (B)	493	388	379	388
E_2	468(E_2)	651	421	408	372
E_1	443(E_1)	613	428	415	389
A_2	469 (A)	691	472	461	394
A_1	572 (A)	818	480	463	416
E_2	722(E_2)	815	588	539	644
B_2	808 (B)	863	641	577	743
E_1	875(E_1)	959	684	621	746
E_2	1246(E_2)	1144	1006	1225	1148
A_2	1314 (A)	1282	1009	1272	1042
E_1	1317(E_1)	1287	1009	1271	1041
B_1	1304 (B)	1243	1021	1282	1065

*Present address: Infineon Technologies, Am Campeon 1-12, 85579 Neubiberg, Germany.
[1] J. Hutter and A. Curioni, ChemPhysChem **6**, 1788 (2005).
[2] Y. Sugita and Y. Okamoto, Chem. Phys. Lett. **314**, 141 (1999).
[3] J. Tersoff, Phys. Rev. Lett. **56**, 632 (1986).
[4] A. Yasukawa, JSME Int. J., Ser. A **39**, 313 (1996).
[5] Y. Umeno, T. Kitamura, K. Date, M. Hayashi, and T. Iwasaki, Comput. Mater. Sci. **25**, 447 (2002).
[6] F. de Brito Mota, J. F. Justo, and A. Fazzio, Phys. Rev. B **58**, 8323 (1998).
[7] F. de Brito Mota, J. F. Justo, and A. Fazzio, J. Appl. Phys. **86**, 1843 (1999).
[8] J. Tersoff, Phys. Rev. B **38**, 9902 (1988).
[9] J. Tersoff, Phys. Rev. B **39**, R5566 (1989).
[10] F. H. Stillinger and T. A. Weber, Phys. Rev. B **31**, 5262 (1985).
[11] R. Biswas and D. R. Hamann, Phys. Rev. B **36**, 6434 (1987).
[12] E. Kaxiras and K. C. Pandey, Phys. Rev. B **38**, R12736 (1988).
[13] M. Z. Bazant, E. Kaxiras, and J. F. Justo, Phys. Rev. B **56**, 8542 (1997).
[14] J. F. Justo, M. Z. Bazant, E. Kaxiras, V. V. Bulatov, and S. Yip, Phys. Rev. B **58**, 2539 (1998).
[15] C. L. Allred, X. Yuan, M. Z. Bazant, and L. W. Hobbs, Phys. Rev. B **70**, 134113 (2004).
[16] B. W. Dodson, Phys. Rev. B **35**, 2795 (1987).
[17] J. Tersoff, Phys. Rev. B **37**, 6991 (1988).
[18] S. von Alfthan, A. Kuronen, and K. Kaski, Phys. Rev. B **68**, 073203 (2003).
[19] Y. Tu, J. Tersoff, G. Grinstein, and D. Vanderbilt, Phys. Rev. Lett. **81**, 4899 (1998).
[20] B. W. H. van Beest, G. J. Kramer, and R. A. van Santen, Phys. Rev. Lett. **64**, 1955 (1990).
[21] S. Tsuneyuki, M. Tsukada, H. Aoki, and Y. Matsui, Phys. Rev. Lett. **61**, 869 (1988).
[22] P. Tangney and S. Scandolo, J. Chem. Phys. **117**, 8898 (2002).
[23] T. Watanabe, H. Fujiwara, H. Noguchi, T. Hoshino, and I. Ohdomari, Jpn. J. Appl. Phys., Part 2 **38**, L366 (1999).
[24] P. Vashishta, R. K. Kalia, J. P. Rino, and I. Ebbsjö, Phys. Rev. B **41**, 12197 (1990).
[25] E. Demiralp, T. Çağin, and W. A. Goddard III, Phys. Rev. Lett. **82**, 1708 (1999).
[26] A. K. Rappé and W. A. Goddard III, J. Phys. Chem. **95**, 3358 (1991).
[27] R. A. Jackson and C. R. A. Catlow, Mol. Simul. **1**, 207 (1988).
[28] B. P. Feuston and S. G. Garofalini, J. Phys. Chem. **89**, 5818 (1988).
[29] B. Vessal, M. Amini, D. Finchman, and C. R. A. Catlow, Philos. Mag. B **60**, 753 (1989).
[30] J. Horbach and W. Kob, Phys. Rev. B **60**, 3169 (1999).
[31] D. Herzbach, K. Binder, and M. H. Muser, J. Phys. Chem. **123**, 1 (2005).
[32] A. C. T. van Duin, A. Strachan, S. Stewman, Q. Zhang, X. Xu, and W. A. Goddard III, J. Phys. Chem. A **107**, 3803 (2003).
[33] K. Tatsumura, T. Watanabe, D. Yamasaki, T. Shimura, M. Umeno, and I. Ohdomari, Jpn. J. Appl. Phys., Part 1 **42**, 7250 (2003).
[34] K. Tatsumura, T. Watanabe, D. Yamasaki, T. Shimura, M. Umeno, and I. Ohdomari, Jpn. J. Appl. Phys., Part 1 **43**, 492 (2004).
[35] K. O. Ng and D. Vanderbilt, Phys. Rev. B **59**, 10132 (1999).
[36] A. Bongiorno and A. Pasquarello, Appl. Phys. Lett. **83**, 1417 (2003).
[37] Y. Tu and J. Tersoff, Phys. Rev. Lett. **84**, 4393 (2000).
[38] S. Dreiner, M. Schurmann, and C. Westphal, Phys. Rev. Lett. **93**, 126101 (2004).
[39] S. Dreiner, M. Schurmann, and C. Westphal, Phys. Rev. Lett. **94**, 189602 (2005).
[40] A. Bongiorno and A. Pasquarello, Phys. Rev. Lett. **94**, 189601 (2005).
[41] J. A. Wendel and W. A. Goddard III, J. Chem. Phys. **97**, 5048 (1992).
[42] X.-Y. Guo and P. Brault, Surf. Sci. **488**, 133 (2001).
[43] C. L. Rountree, R. K. Kalia, E. Lidorikis, A. Nakano, L. V. Brutzel, and P. Vashishta, Annu. Rev. Mater. Res. **32**, 377 (2002).
[44] X. T. Su and S. H. Garofalini, J. Appl. Phys. **97**, 113526 (2005).
[45] P. Vashishta, A. Nakano, R. K. Kalia, and I. Ebbsjö, Mater. Sci. Eng., B **37**, 56 (1996).
[46] M. E. Bachlechner, A. Omeltchenko, A. Nakano, R. K. Kalia, P. Vashishta, I. Ebbsjö, and A. Madhukar, Phys. Rev. Lett. **84**, 322 (2000).
[47] CAChe Materials Explorer, Copyright Fujitsu Limited, 2001, http://www.cachesoftware.com/materialsexplorer/index.shtml
[48] N. Troullier and J. L. Martins, Phys. Rev. B **43**, 1993 (1991).
[49] J. P. Perdew, K. Burke, and M. Ernzerhof, Phys. Rev. Lett. **77**, 3865 (1996).
[50] CPMD, Copyright IBM Corp. 1990–2005 and MPI für Festkörperforschung, Stuttgart, Germany, 1997–2001.
[51] J. Hutter, H. P. Lüthi, and M. Parrinello, Comput. Mater. Sci. **2**, 244 (1994).
[52] R. W. Hockney, Methods Comput. Phys. **9**, 136 (1970).
[53] D. Fischer, A. Curioni, S. Billeter, and W. Andreoni, Phys. Rev. Lett. **92**, 236405 (2004).
[54] D. C. Liu and J. Nocedal, Math. Program. **45**, 503 (1989).
[55] T. Rowan, Ph.D. thesis, Department of Computer Sciences, University of Texas at Austin, 1990.
[56] H. Sun and D. Rigby, Spectrochim. Acta, Part A **53**, 1301 (1997).
[57] H. Sun, J. Phys. Chem. B **102**, 7338 (1998).
[58] N. R. Keskar and J. R. Chelikowsky, Phys. Rev. B **48**, 16227 (1993).
[59] M. Catti, B. Civalleri, and P. Ugliengo, J. Phys. Chem. B **104**, 7259 (2000).
[60] A. P. Mirgorodsky, M. I. Baraton, and P. Quintard, Phys. Rev. B **48**, 13326 (1993).
[61] W.-Y. Ching, Y.-N. Xu, J. D. Gale, and M. Rühle, J. Am. Ceram. Soc. **81**, 3189 (1998).
[62] D. Fischer, A. Curioni, S. R. Billeter, and W. Andreoni, Appl. Phys. Lett. **88**, 012101 (2006).
[63] W. Andreoni, A. Curioni, D. Fischer, C. A. Pignedoli, and S. R. Billeter, in *Defects in High-k Gate Dielectric Stacks*, edited by E. Gusev, NATO Science Series (Springer, Berlin, 2006), Vol. II/220, p. 203.
[64] G. A. Lager, J. D. Jorgensen, and F. J. Rotella, J. Appl. Phys. **53**, 6751 (1982).
[65] R. W. G. Wyckoff, *Crystal Structures*, 2nd ed. (Interscience, New York, 1963), Vol. 1.
[66] J. J. Pluth, J. V. Smith, and J. Faber, J. Appl. Phys. **57**, 1045 (1985).
[67] S. Wild, P. Grieveson, and K. H. Jack, in *Special Ceramics*, edited by P. Popper (British Ceramic Research Association, Stoke-on-Trent, 1972), Vol. 5, p. 385.

[68] A. Navrotsky, in *Mineral Physics & Crystallography, Handbook of Physical Constants*, edited by T. J. Ahrens (American Geophysical Union, Washington, D.C., 1995), pp. 18–29.
[69] F. Gervais and B. Piriou, Phys. Rev. B **11**, 3944 (1975).
[70] J. D. Masso, C. Y. She, and D. F. Edwards, Phys. Rev. B **1**, 4179 (1970).
[71] N. Wada, S. A. Solin, J. Wong, and S. Prochazka, J. Non-Cryst. Solids **43**, 7 (1981).